Journal of Catalysis 276 (2010) 24–37

Contents lists available at ScienceDirect

Journal of Catalysis

journal homepage: www.elsevier.com/locate/jcat

Stability and performance of cation vacant $Fe_{3-x-y}V_x\square_yO_4$ spinel phase catalysts in methanol oxidation

Robert Häggblad [a,1], Staffan Hansen [b], L. Reine Wallenberg [b], Arne Andersson [a,*]

[a] Department of Chemical Engineering, Lund University, Chemical Center, P.O. Box 124, SE-221 00 Lund, Sweden
[b] Division of Polymer and Materials Chemistry, Department of Chemistry, Lund University, Chemical Center, P.O. Box 124, SE-221 00 Lund, Sweden

ARTICLE INFO

Article history:
Received 25 May 2010
Revised 18 August 2010
Accepted 19 August 2010

Keywords:
Selective oxidation
Methanol
Formaldehyde
$Fe_{3-x-y}V_x\square_yO_4$ catalysts
Fe–V–O spinel-type phases
Volatility
HRTEM
In situ XANES
XPS
XRD

ABSTRACT

A series of spinel-type Fe–V–O phases were prepared with V/Fe atomic ratios ranging from 0 to 1 and were used for methanol oxidation to formaldehyde. X-ray powder diffraction shows that the basic spinel-type structure is retained after use of the samples in methanol oxidation. Compared with the freshly prepared samples, in- and ex situ analyses of the samples with XANES show that both V and Fe are oxidized under influence of methanol oxidation, where octahedrally coordinated V^{3+} partially is oxidized to V^{4+}. Simultaneously, partial oxidation occurs of Fe^{2+} in tetrahedral and octahedral coordinations to form Fe^{3+} species. XPS reveals that in general the surfaces with predominantly V^{5+} and Fe^{3+} species are more oxidized compared to the bulk. Besides XRD, HRTEM imaging confirms that the basic spinel type structure is stable in methanol oxidation. Consequently, the structure is very flexible allowing the cations to change oxidation state by forming cation vacancies without structural breakdown. All preparations show activity of similar magnitude although great differences in selectivity to formaldehyde. The best performing spinel catalyst is poor in vanadium with a V/Fe ratio of 1/14, indicating that isolated vanadia moieties perform better than polymeric vanadia structures. The stable and flexible structure makes the spinel-type Fe–V–O catalysts an interesting alternative to the presently used industrial catalyst consisting of a mixture of MoO_3 and ferric molybdate. Opposed to the industrial catalyst, which suffers from Mo volatilization, the spinel samples show no measurable volatilization of vanadium.

1. Introduction

With a production of almost 35 million tons per year in 2008 expressed as a 37 wt.% water solution [1], formaldehyde is a key intermediate in the chemical industry for the production of a wide variety of important products that are used in our everyday life such as adhesives for panels, coatings, plastics and much more [2,3]. Today, formaldehyde is produced by two competing processes, the silver and the oxide process operating with a methanol concentration respectively above (36–40%) and below (8.5–10%) the explosive limit of methanol [2]. Depending on the operating conditions, the overall plant yield to formaldehyde in the silver and the oxide process is 86–90% and 90–93%, respectively [2–4]. As a consequence of the methanol price has almost been doubled over the last five years, the more selective oxide process has gained market shares over the silver process [5].

The $MoO_3/Fe_2(MoO_4)_3$ catalyst used in the oxide process is in most aspects superb, showing very high selectivity to formaldehyde (>93%) at almost complete methanol conversion. However, at the reaction conditions the catalyst suffers from deactivation due to volatilization of molybdenum, which results in lower activity and selectivity to formaldehyde [6–10]. Consequently, the catalyst has to be replaced regularly depending on the reaction conditions [10]. Since higher temperature and methanol partial pressure facilitate the volatilization of molybdenum [6], higher plant capacity is difficult to achieve by increasing the inlet concentration of methanol. Therefore, alternative catalysts showing lower volatilization rate of the active components are of interest [11]. However, although low volatility is important, also other issues are essential when considering alternative catalysts for use in industrial plants. As the methanol cost represents more than 90% of the production costs [12], lower selectivity compared to that obtained by the commercial $MoO_3/Fe_2(MoO_4)_3$ catalyst is not economically feasible. Furthermore, due to environmental and health concerns it is desirable to restrict the amount of harmful substances in the catalyst.

Vanadium-based catalysts have been studied both in supported and unsupported forms [11,13–25]. Among the vanadates, $FeVO_4$ is one of the most promising candidates with a reported selectivity to formaldehyde between 90% and 95.4% at high methanol conversion at 300 °C [20,25]. Besides showing high selectivity, the volatility of the vanadium from the catalyst is much lower than that of

* Corresponding author. Fax: +46 46 149156.
E-mail address: Arne.Andersson@chemeng.lth.se (A. Andersson).
[1] Present address: Formox AB, SE-284 80, Perstorp, Sweden.

0021-9517/$ - see front matter © 2010 Elsevier Inc. All rights reserved.
doi:10.1016/j.jcat.2010.08.012

molybdenum from commercial $MoO_3/Fe_2(MoO_4)_3$-type catalysts. After five days at 300 °C in an atmosphere of 10% methanol and 10% oxygen, the vanadium and molybdenum loss was 5.7% and 35.7%, respectively [25]. However, although $FeVO_4$ is a promising catalyst with regard to both the selectivity and the volatility, the concentration of toxic vanadium is high, making it environmentally less attractive compared to the $MoO_3/Fe_2(MoO_4)_3$ catalyst. Therefore, it is of interest to decrease the amount of vanadium in the catalyst. A common approach to reduce the amount of active phase is to use supports with a layer of active oxide in the monolayer range. In our previous work [25], besides showing lower selectivity to formaldehyde than bulk $FeVO_4$, vanadium losses between 42% and 96% were observed from α-Al_2O_3, SiO_2 and TiO_2 with 1 and 5 theoretical layers of Fe–V–oxide, making them inappropriate as catalysts for methanol oxidation. Another approach to decrease the amount of vanadium is to use bulk phases with low vanadium content. In a previous work [23], during the catalysis at 350 °C we observed transformation of $FeVO_4$ into a cation vacant $Fe_{1.26}V_{1.26}O_4$ spinel-type structure. For such spinels, it has been reported possible to vary the molar V/Fe ratio as much as between 0 and 0.67 [26].

In this study, we have prepared and measured the catalytic performance in methanol oxidation of a series of catalysts with cation vacant $Fe_{3-x-y}V_x\square_yO_4$ spinel-type structures where □ denotes a cation vacancy. Moreover, the catalysts have been characterized by X-ray diffraction (XRD), high-resolution transmission electron microscopy (HRTEM), temperature-programmed oxidation (TPO), X-ray photoelectron spectroscopy (XPS) and in situ XANES (X-ray absorption near edge structure) spectroscopy.

2. Experimental

2.1. Catalyst preparation

A series of $Fe_{3-x-y}V_x\square_yO_4$ catalysts with $x = 0$, 0.06, 0.19, 0.97 and 1.37 were prepared by precipitation from a homogenous water solution containing the metal ions. In the spinel structure, cation vacancies □ are formed when the average cation valence exceeds +8/3 [27], and the number of vacancies is determined by the charge balance. A homogenous solution of the metal salts was prepared from two separate water solutions, a 0.04 M NH_4VO_3 (Merck) solution and a 0.5 M solution of $Fe(NO_3)_3{\cdot}9H_2O$ (Merck). The two well-stirred solutions were mixed together in the desired proportions and were then homogenized by lowering the pH to 1.0 by adding 3 M HNO_3. A solid precipitated when the pH was rapidly raised to 4.0 by the addition of 3 M NH_3. Particle coarsening was carried out to facilitate the recovery of the particles [28] by heating the turbid solution for 2 h at 50 °C with maintained stirring. The particles were separated by centrifugation (3000 rpm, 3 min) and then washed three times with water, acetone and again water, respectively. Finally, the samples were dried for 16 h at 80 °C and subsequently reduced for 15 h at 450 °C in a H_2/H_2O/Ar mixed atmosphere. In Table 1 are given the notation of the catalysts, their composition as prepared and the specific surface area before and after five days use of the samples in methanol oxidation at the conditions described in Section 2.3.

2.2. Activity measurements

The prepared catalysts were tested for methanol oxidation to produce formaldehyde in a stainless steel reactor with an inner diameter of 6 mm, operating at isothermal conditions and atmospheric pressure. To improve the heat transfer, the reactor was embedded in an aluminum block placed in a tube furnace. For the measurements, the catalyst sample was ground into fine powder and pressed into tablets, which were crushed and sieved to particles with diameters in the range 0.250–0.425 mm. The reactor was loaded with the desired amount of catalyst. The catalyst was heated up to the reaction temperature in a flow of 80 ml/min N_2. When the reaction temperature 300 °C was reached, a flow of 10 ml/min of O_2 and 10 ml/min gaseous methanol was added to the flow of nitrogen.

Table 1
Sample composition and specific surface area of prepared catalysts (fresh) and after 5 days operation at 300 °C in a stream of nitrogen with 10% oxygen and 10% methanol (used).

Sample	Composition[a]	Specific surface area (m^2/g)	
		Fresh samples	Used samples
$FeVO_4$	$FeVO_4$	15.2	16.8
$Fe_{1.5}V_{1.5}$	$Fe_{1.37}V_{1.37}\square_{0.26}O_4$	18.2	15.8
$Fe_{2.0}V_{1.0}$	$Fe_{1.94}V_{0.97}\square_{0.09}O_4$	14.1	11.7
$Fe_{2.8}V_{0.2}$	$Fe_{2.67}V_{0.19}\square_{0.14}O_4$	8.0	6.9
$Fe_{2.94}V_{0.06}$	$Fe_{2.90}V_{0.06}\square_{0.04}O_4$	5.6	4.2
$Fe_{3.0}V_{0.0}$	$Fe_{2.99}V_0\square_{0.01}O_4$	5.3	N.D.[b]

[a] As determined by TPO on fresh samples (see Section 2.3).
[b] Not determined.

The feed concentrations of methanol and oxygen, 10 vol.% each, are the same as those presently being used in many plants [29]. In the plants, the feed also contains about 2.5% water, since oxygen poor gas from the absorber is recirculated to the inlet to be mixed with air and methanol to give the desired methanol and oxygen concentrations in the feed [2]. The water content varies with the location of the plant, the absorber temperature and the climate. Since water in the feed slows down the reaction rate, the reaction temperature or the catalyst load plan is adjusted in order to obtain the desired conversion. Concerning the flammability limits for methanol–oxygen–inert gas mixtures, it is worth to point out that the feed composition that we have used is at the borderline of the flammability region [30], but experiments have shown that a feed with 10% methanol is safe to operate with an oxygen content up to about 13 vol.% since no propagation can occur when the gas flows through a packed-bed reactor [12].

Catalytic data are presented as activities and selectivities. The selectivities presented are those for high methanol conversion, which are the most interesting from an applied point of view. In these measurements, depending on the activity of the catalyst, the amount of catalyst used was in the range 0.14–1.0 g. The activities presented are the conversion rates of methanol measured at low conversion, thus corresponding approximately to reaction rates for the defined inlet conditions. In these measurements, a stainless steel reactor with an internal diameter of 1 mm was used. The amount of catalyst charged was about 20–30 mg in most cases.

Methanol, formaldehyde (FA), dimethyl ether (DME), methyl formate (MF), dimethoxymethane (DMM) and CO_2 were analyzed online on a gas chromatograph equipped with a Haysep C column and both an FID and a TCD detector. CO was analyzed online on an IR instrument (Rosemount Binos 100).

2.3. Catalyst characterization

The specific surface areas of the catalysts were measured on a Micromeritics Flowsorb 2300 instrument. The single point BET method was used with adsorption of nitrogen at liquid nitrogen temperature and subsequent desorption at room temperature. All samples were degassed at 150 °C for 24 h before analysis.

Temperature-programmed oxidation (TPO) experiments were performed on a Micromeritics TPD/TPR 2900 equipped with a TCD detector. The oxidations were made from 30 °C to 670 °C with a heating rate of 5 °C/min and a gas composition of 5% O_2 in He. For each sample, the oxidation profile returned to the baseline,

confirming the cations being oxidized to their highest oxidation states, i.e. V^{5+} and Fe^{3+}. From the oxygen uptake determined by integration of the profiles, the average oxidation number of the cations in each sample and hence the number y of cation vacancies in the formula $Fe_{3-x-y}V_x\square_yO_4$ were calculated.

X-ray powder diffraction (XRD) analysis was performed on a Seifert XRD 3000 TT diffractometer using Ni-filtered Cu Kα radiation and a rotating sample holder. Data were collected between 5° and 80° 2θ in steps of 0.1° (2.0 s/step). The samples were analyzed using the freeware PowderCell 2.4 written by Kraus and Nolze, Berlin. In the Rietveld refinements, the following parameters were varied: scaling factor, zero shift and overall temperature factor, as well as lattice, background and peak width parameters, while the atomic positions were kept fixed. Crystal structure data were taken from Ref. [31] for $FeVO_4$, from Ref. [32] for the Fe_3O_4 magnetite-type structures and from Ref. [33] for the γ-Fe_2O_3 maghemite-type structures. The spinel-type structure of magnetite Fe_3O_4 [32] was used as a starting model in the calculations. A fully disordered cation distribution was used in the initial refinements by least squares. After convergence of the calculations, two models with as much V as possible in octahedral or tetrahedral sites, respectively, were tested. Due to low degree of crystallinity, no refinement could be performed on the $FeVO_4$, $Fe_{1.5}V_{1.5}$ and $Fe_{2.0}V_{1.0}$ catalysts after they had been used for 5 days in methanol oxidation. Instead, the lattice parameter of a spinel-type structure was adjusted by comparison of experimental and calculated patterns in order to obtain the calculated peaks at the observed scattering angles 2θ.

After activity measurement and phase determination by XRD, the $Fe_{1.5}V_{1.5}$ and $Fe_{2.8}V_{0.2}$ catalysts were selected for analysis by HRTEM. The employed electron microscope was a JEOL 3000F with a point resolution of 0.16 nm in conventional transmission mode. Particle sizes were determined from overview images and the structure and composition of individual crystallites by HRTEM imaging, selected area electron diffraction (SAD) and X-ray energy dispersive spectrometry (XEDS).

XPS analysis was performed on a PHI 5500 XPS instrument using monochromatic Al Kα radiation. Powder samples were placed on a conducting and sticky tape. To minimize the effects of sample charging, the samples were charge neutralized by electrons. Quantifications of the elements were made using the PC-ACCESS software and a Shirley function for the background. The C 1s peak was used as an energy reference and was set to a binding energy of 285.0 eV. Data used for the quantifications were collected using a sufficient amount of sample to exclude any signal from the underlying carbon film. In order to quantify the oxidation state distribution of V, deconvolution of the V $2p_{3/2}$ peak into single or multiple Gaussian curves was made using the OriginPro 7.5 software. The fitting was performed on the low energy side of the peak maximum, which is symmetric for a single valence state and asymmetric when multiple valences are present. The energy position and the full width half maximum (FWHM) values were carefully controlled during the fitting and were allowed to vary from the average not more than ±0.2 eV and ±0.05 eV, respectively.

The XANES measurements were carried out at the I811 beamline in Maxlab (Lund University) using a Si(1 1 1) double crystal monochromator and three ionization chambers. Spectra of the Fe *K*- and V *K*-edges were recorded in transmission mode using Fe (7110.75 eV) and V (5463.76 eV) metal foils as energy references [34]. The sample was placed in between the first and the second ionization chambers, and the reference was placed before the third chamber. To obtain an optimal absorption signal, the sample was diluted with boron nitride. Since no distinct peak is displayed in the derivative spectra of neither the V *K*- nor the Fe *K*-edge, the main edge positions reported are the energies at half the edge jump ($E_{1/2}$) in the normalized spectra.

In situ XANES spectra were recorded in transmission mode on 53- to 106-μm particles using the homemade reaction cell displayed in Fig. 1. To obtain conditions similar to an isothermal plug-flow reactor, the cell was constructed of aluminum, and the gas was passing through the catalytic bed (width × depth = 10 × 1 mm). The height of the bed was approximately 10–15 mm. The cell was sealed by graphite seals, and kapton windows were positioned on each side of the catalytic bed. A thermocouple type K was mounted in the aluminum block close to the catalytic bed, and the cell was heated with two 100-W cartridge heaters positioned on each side of the bed. To prevent heat leakage and protect the surrounding equipment, the cell was mounted in an insulated cover box. Before starting the measurements, the cell was heated from room temperature to the reaction temperature 300 °C under a flow of 16 ml/min Ar. Typically, five XANES spectra were recorded before adding 2 ml/min O_2 and 2 ml/min gaseous methanol to the flow of Ar. During reaction, Quick-XAFS spectra were recorded from 5413 to 7261 eV using a V metal foil as energy reference.

In order to obtain information about the valence and the coordination of V and Fe, pre-edge analysis of both the V *K*- and the Fe *K*-spectra were performed. The procedure is very similar to that being described earlier for both the V *K*- [35–37] and the Fe *K* pre-edge [38,39]. A background-subtracted pre-edge feature was obtained from the normalized XANES spectrum by subtracting the contribution from the main edge using a spline function to interpolate the background from several eV before to a few eV after the pre-edge. The background-subtracted pre-edge was deconvoluted into Gaussian curves using the software OriginPro 7.5. The fitting parameters such as number of peaks, position and FWHM were carefully controlled to mimic as good as possible the fitted results presented in the literature [35,37–39]. From deconvolution of the

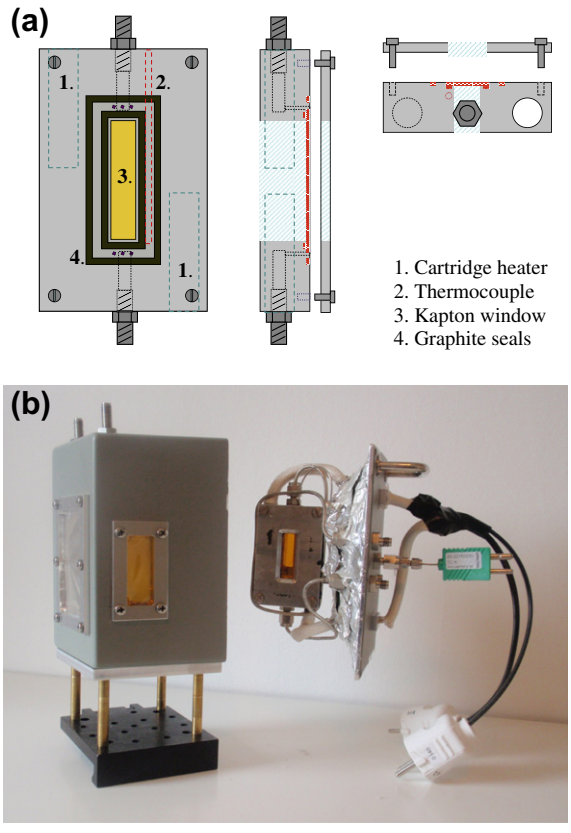

Fig. 1. (a) Drawing and (b) image of the reaction cell that was used for collecting in situ XANES spectra. To prevent heat leakage and protect the surrounding equipment, the cell was mounted on the insulated cover box seen in b.

V *K* pre-peak, the centroid position (in this case the center of peak area) and the normalized intensity were determined and compared with data for a number of reference compounds with known valence and coordination [35,37,40,41]. Since the pre-peak intensity depends on the type of monochromator crystal [37], in relevant cases data for reference compounds were adjusted from Si(2 2 0) and Si(3 1 1) to Si(1 1 1) according to the difference reported in Refs. [35,37]. For comparison with the reference compounds taken from the literature, the V *K*-edge value used for the V metal foil was set to 5465 eV.

To study the volatility of vanadium in methanol oxidation, a multitube reactor was used where about 20–30 mg of each catalyst was treated for 5 days at 300 °C in a flow of nitrogen with 10% methanol and 10% oxygen. The amount of catalyst was selected to assure differential conversion of methanol (<12%), corresponding to reactor inlet conditions. After the treatment, the catalysts were cooled down to room temperature under flowing nitrogen before being subjected to elemental analysis with ICP-AES (inductively coupled plasma-atomic emission spectrometry). Also, the same samples were then activity tested and characterized with XRD, HRTEM, XEDS, XANES and XPS after thorough grinding and mixing. These samples are designated used samples.

3. Results

3.1. X-ray diffraction

The catalysts were characterized by XRD both as synthesized and after use in methanol oxidation, with the samples designated fresh and used, respectively. As shown in the left column in Fig. 2, both the fresh $FeVO_4$ and the series of $Fe_{3-x-y}V_x\square_yO_4$ samples are phase pure since no additional peaks can be observed except the ones being characteristic for triclinic $FeVO_4$, JCPDS 25-418 [42] respectively Fe_3O_4-related spinel type of phases, JCPDS 19-629 [42]. In Table 2 are summarized the results of the Rietveld analysis. The experimental patterns are best fitted with vanadium being positioned in octahedral sites, which agree with previous observations [26,43]. Compared with the fresh spinel samples with low content of V ($Fe_{2.94}V_{0.06}$, $Fe_{2.8}V_{0.2}$), the diffraction peaks of the samples with high V contents ($Fe_{2.0}V_{1.0}$, $Fe_{1.5}V_{1.5}$) are considerably broader, indicating decreasing crystallite size as the V content increases. This indication is supported by the BET results in Table 1 showing increasing specific surface area as the V concentration increases.

It has been demonstrated that the original triclinic $FeVO_4$ phase only to a small extent remains after 16 h use in methanol oxidation at 350 °C and with 6% methanol concentration [23]. Instead, a spinel type of structure is formed, which is related to the structures of Fe_3O_4 and γ-Fe_2O_3. As displayed in Fig. 2, an even more complete transformation of $FeVO_4$ is observed in this study using higher methanol concentration. In the diffractogram of the used sample, no sign of any peaks belonging to the original triclinic phase can be detected. Also $Fe_{1.5}V_{1.5}$ undergoes a significant transformation during the catalysis. Although the bulk phase remains of spinel type, the X-ray diffraction pattern of the used sample is different from that of the fresh sample. The intensity ratios between the peaks differ, the peaks are slightly broader, and the catalyst is less crystalline as revealed by the relatively low intensity of the diffraction peaks. Furthermore, comparing the diffraction pattern (Fig. 2) and the lattice parameter *a* (Table 2) of the used $Fe_{1.5}V_{1.5}$ catalyst with the pattern and parameter of the used $FeVO_4$ clearly shows

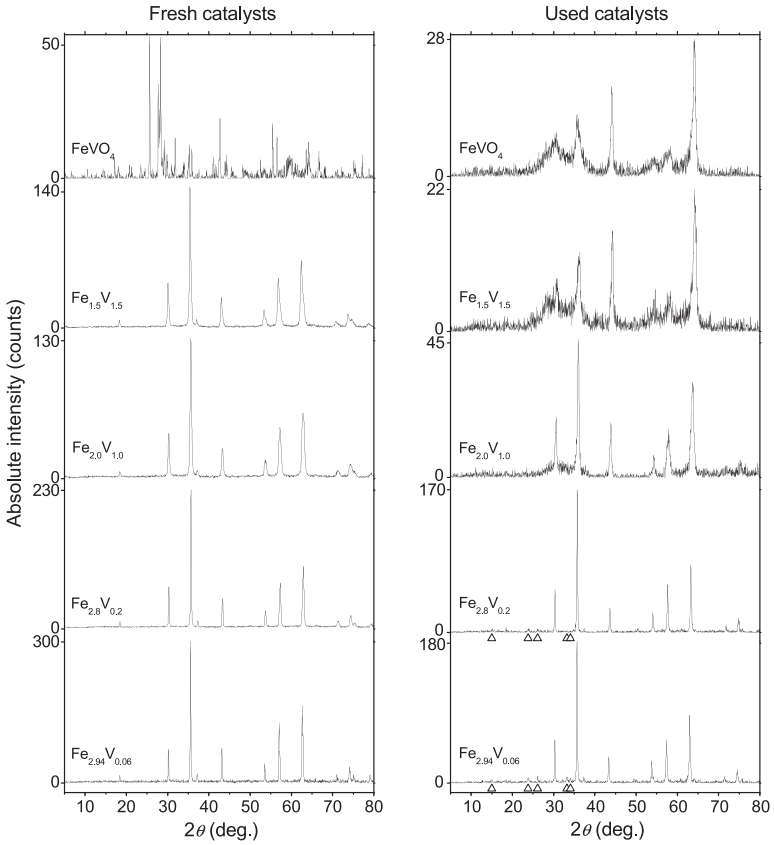

Fig. 2. X-ray diffraction patterns of the $FeVO_4$ and $Fe_{3-x-y}V_x\square_yO_4$ catalysts as prepared (left) and after 5 days in methanol oxidation (right). (Δ) Reflections from a maghemite-type structure.

Table 2
Crystal structure analysis of the catalysts.

Sample	Fresh	Used
$FeVO_4$	Triclinic a = 6.708, b = 8.051, c = 9.331 Å α = 96.7, β = 106.6, γ = 101.5°	Spinel-type, face-centered cubic[a] a = 8.25 Å[a]
$Fe_{1.5}V_{1.5}$	Spinel-type, face-centered cubic[b] a = 8.415 Å	Spinel-type, face-centered cubic[a] a = 8.24 Å[a]
$Fe_{2.0}V_{1.0}$	Spinel-type, face-centered cubic[b] a = 8.374 Å	Spinel-type, face-centered cubic[a] a = 8.27 Å[a]
$Fe_{2.8}V_{0.2}$	Spinel-type, face-centered cubic[b] a = 8.370 Å	Spinel-type, primitive cubic[c] a = 8.288 Å
$Fe_{2.94}V_{0.06}$	Spinel-type, face-centered cubic a = 8.396 Å	Spinel-type, primitive cubic[c] a = 8.347 Å (plus traces of hematite)

[a] Not refined by least squares.
[b] V in octahedral sites.
[c] Metal vacancies in octahedral sites.

the resemblance between the two catalysts. Thus, although the bulk phases of the fresh catalysts are different, the structure and composition are similar after the samples being used in methanol oxidation. Fig. 2 also shows that substitution of Fe for V increases the stability of the bulk phase, as revealed by the observation that the differences between the diffraction patterns of fresh and used catalysts become smaller as the V concentration decreases.

In the diffraction patterns of the used $Fe_{2.8}V_{0.2}$ and $Fe_{2.94}V_{0.06}$, weak extra reflections are present in addition to the main peaks corresponding to a spinel-type phase. In the sample $Fe_{2.8}V_{0.2}$, all the major and minor reflections could be refined as a maghemite-type (γ-Fe_2O_3-type) structure, which is a spinel structure with ordered cation vacancies [33]. In the used $Fe_{2.94}V_{0.06}$, the extra reflections are stronger, and most of them could again be refined using the maghemite-type structure, while some remaining weak reflections could be identified as α-Fe_2O_3 [44]. The fit could be improved by the introduction of cation vacancies in the octahedral sites.

For the spinel-type catalysts, the data in Table 2 show decreased lattice parameter of the used catalyst when compared to the fresh one. For the pure iron oxides, the lattice parameter a is equal to 8.39 Å for the spinel-type magnetite $Fe^{II}Fe^{III}_2O_4$ [32] and 8.34 Å for the cation-deficient maghemite $Fe^{III}_{2.67}\square_{0.33}O_4$ (γ-Fe_2O_3) [33]. The spinel-type phases in the fresh samples exhibit a lattice parameter in the range 8.37–8.42 Å, without any clear trend with respect to the degree of substitution of iron with V. For the phase in the used catalysts, the a parameter is 8.24–8.35 Å, indicating an oxidation during the reaction.

3.2. HRTEM

Two samples, $Fe_{1.5}V_{1.5}$ and $Fe_{2.8}V_{0.2}$, in fresh and used form were selected for investigation by TEM. The particle sizes are quite similar within the composition class, as shown in Fig. 3. For

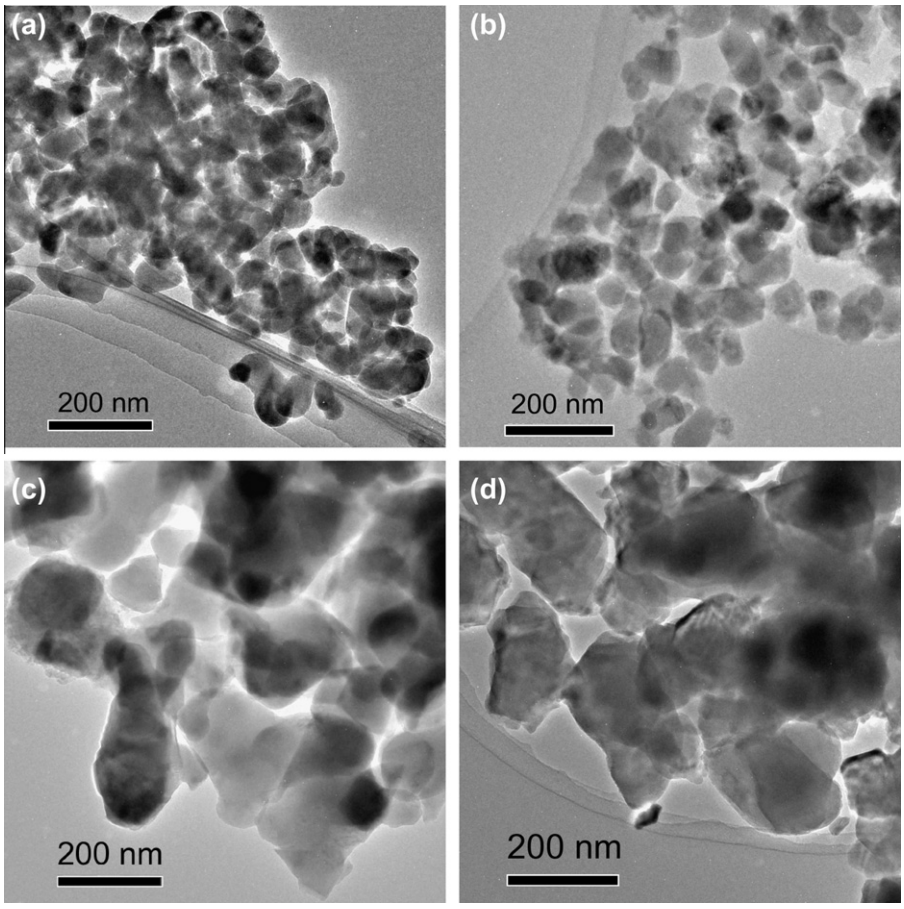

Fig. 3. Overview of TEM images at low magnification showing typical particle sizes and morphology before and after use of the samples in methanol oxidation. (a) $Fe_{1.5}V_{1.5}$ fresh, (b) $Fe_{1.5}V_{1.5}$ used, (c) $Fe_{2.8}V_{0.2}$ fresh and (d) $Fe_{2.8}V_{0.2}$ used. The magnification is the same in all images.

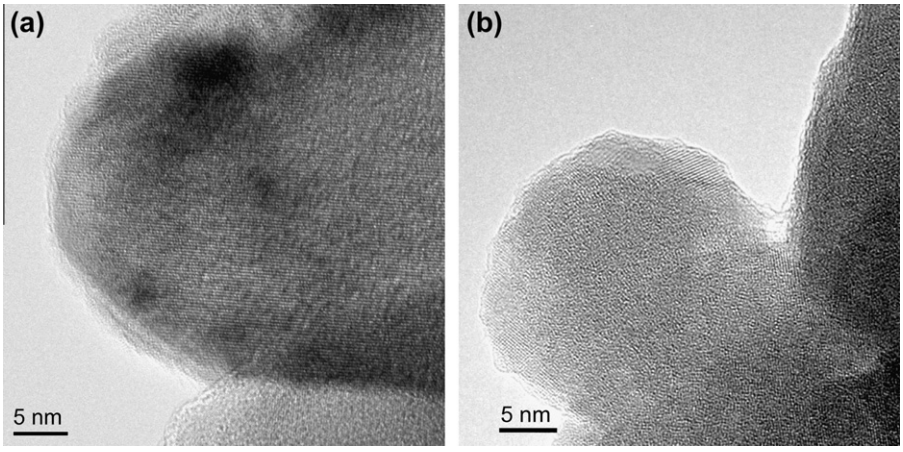

Fig. 4. HRTEM images of the $Fe_{1.5}V_{1.5}$ sample (a) before and (b) after methanol oxidation. The degree of crystallinity appears to be lower in the used sample.

$Fe_{1.5}V_{1.5}$, the particle size is in the range 20–120 nm with a smooth and rounded shape, and for $Fe_{2.8}V_{0.2}$ the particles are approximately 100–250 nm and have a more irregular, facetted form due to a higher crystallinity. Compared to the fresh $Fe_{1.5}V_{1.5}$, the corresponding used sample (Fig. 4) has a larger proportion of areas appearing amorphous with very small crystallites preferentially at the surface, which is consistent with the X-ray data from these two samples.

For the fresh $Fe_{2.8}V_{0.2}$, the crystallites are well defined, and Fig. 5 shows a high-resolution micrograph of a crystallite viewed along the [0 1 1] direction. In the inset, the reciprocal distance to the indexed reflections in the calculated Fourier transform corresponds well with the refined spinel-type structure data in Table 2.

The used $Fe_{2.8}V_{0.2}$, however, shows clear superstructure reflections in many of the recorded electron diffraction patterns from different crystallites, and the HREM images have a weaker herringbone-type contrast superimposed on the spinel sublattice (Fig. 6a–c). Fourier transforms calculated from a small area close to edges of the crystallite (Fig. 6b) reveal that the superstructure is in fact one-dimensional along one of the cubic axes and gives a threefold extension of the axis length. The recorded electron diffraction pattern in Fig. 6c comes from a larger volume, and the apparent two- or three-dimensional superstructure is due to extensive twinning on {1 1 0} planes.

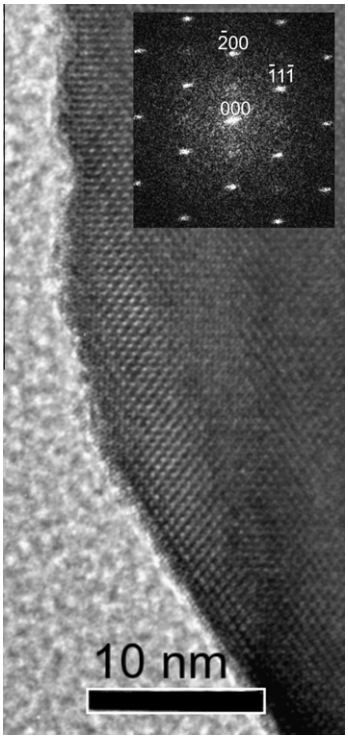

Fig. 5. HRTEM image of freshly prepared $Fe_{2.8}V_{0.2}$. The inset shows the Fourier transform of the image recorded along the [0 1 1] direction of the face-centered unit cell. Distances to the indexed diffraction spots (d_{111} and d_{200} type) correspond to 0.487 and 0.419 nm, respectively, giving $a_0 = 0.837$ nm (Table 2: 0.837 nm, literature data for pure Fe_3O_4 0.8394 nm [32]).

3.3. TPO

In order to determine the oxygen content and obtain information about the valences of Fe and V in the fresh samples, TPO measurements were made. Displayed in Fig. 7 are the TPO profiles of the $Fe_{1.5}V_{1.5}$, $Fe_{2.8}V_{0.2}$ and $Fe_{3.0}V_{0.0}$ samples. The $Fe_{3.0}V_{0.0}$ profile, showing a doublet peak with a maximum intensity at approximately 244 °C and a shoulder at approximately 266 °C, strongly resembles the calorimetric profile recorded by Nivoix et al. during oxidation of nanometric sized magnetite [26]. Both peaks are assigned to the oxidation of divalent Fe at octahedral sites [26]. Two main observations are seen in Fig. 7 when substituting V for Fe. First, when the vanadium concentration is increased, the onset temperature of the oxidation tends to decrease. The decrease in the onset temperature probably is a crystallite size effect, considering the BET (Table 1) and XRD (Fig. 2) results showing increasing specific surface area and decreasing crystallite size, respectively, with increasing V content in the catalyst. The second main observation is that although the oxidation starts at lower temperature when substituting V for Fe, the oxygen consumption at low temperatures (150–300 °C) decreases as revealed by integration of the profiles in Fig. 7. Instead, the oxygen is consumed at higher temperatures resulting for $Fe_{2.8}V_{0.2}$ and $Fe_{1.5}V_{1.5}$ in broad spectral features in the interval 300–450 °C, which is in agreement with calorimetric curves for vanadium-containing magnetite [26]. Moreover, for $Fe_{1.5}V_{1.5}$ two strong peaks are visible at approximately 500 °C and 570 °C, which are due to the formation of $FeVO_4$ [26].

The average valence of the cations and the consequent number of cation vacancies were determined by integration of each TPO spectrum, giving the compositions as shown in Table 1. For $Fe_{3.0}V_{0.0}$, the composition obtained corresponds to stoichiometric magnetite [40]. However, the TPO measurements reveal that both $Fe_{2.8}V_{0.2}$ and $Fe_{1.5}V_{1.5}$ are oxidized magnetites with the element compositions $Fe_{2.67}V_{0.19}\square_{0.14}O_4$ and $Fe_{1.37}V_{1.37}\square_{0.26}O_4$,

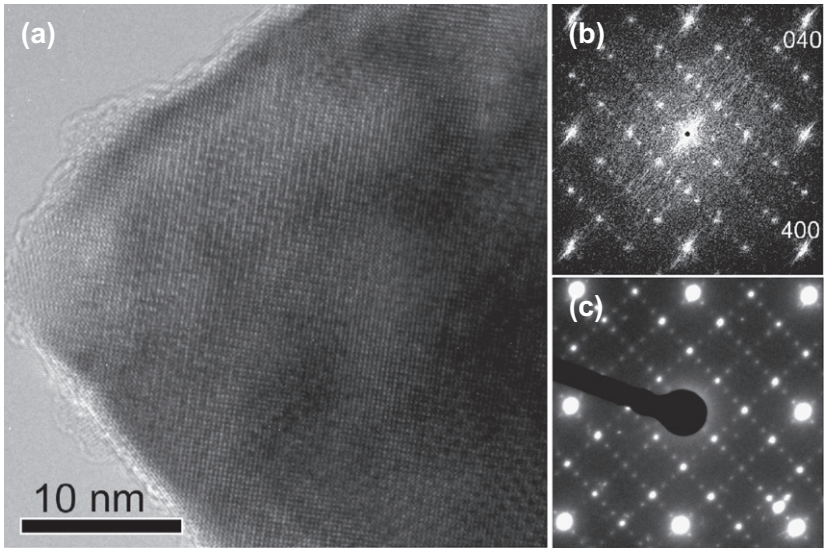

Fig. 6. Imaging of $Fe_{2.8}V_{0.2}$ after use in methanol oxidation. (a) HRTEM image along the ⟨0 0 1⟩ zone axis, (b) FFT of local area, showing one-dimensional threefold superstructure. The viewing direction is determined as [0 0 −1], and marked indices correspond to the cubic spinel structure with the axes 0.84–0.86 nm (Table 2 a_0 = 0.829 nm, literature data for pure γ-Fe_2O_3 0.834 nm [33]), and (c) recorded selected area diffraction pattern (SAD) of the whole particle, showing the effect of twinning in larger grains.

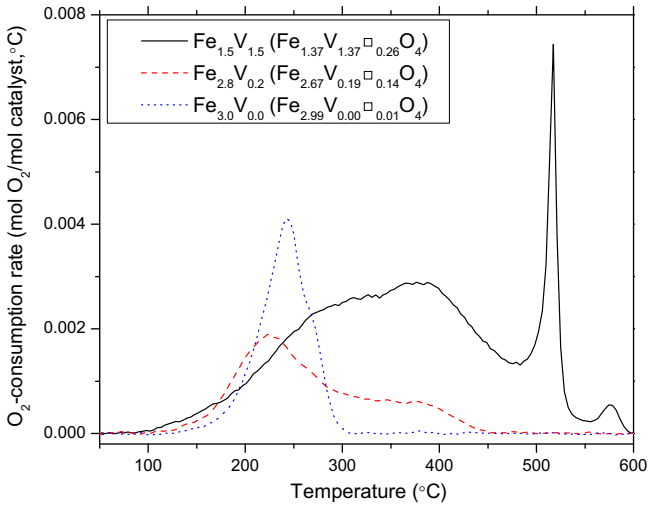

Fig. 7. TPO profiles of the fresh $Fe_{1.5}V_{1.5}$, $Fe_{2.8}V_{0.2}$ and $Fe_{3.0}V_{0.0}$ samples. The oxidations were made between 30 °C and 670 °C with a heating rate of 5 °C/min and a gas composition of 5 vol.% O_2 in He. From the oxygen uptake, the average oxidation state of the cations and number of cation vacancies were calculated, which data are given in Table 1.

respectively, corresponding to an average cation valence of +2.79 and +2.92, respectively. In comparison, the composition of pure maghemite (γ-Fe_2O_3) is $Fe_{2.67}\square_{0.33}O_4$. According to the data in Table 1, there is a trend that the vacancy content of the unit cell increases with increase in the vanadium content. The trend is in line with V unlike Fe can have a valence above +3.

3.4. In situ XANES

In order to on stream observe changes in valence and coordination of Fe and V, in situ XANES experiments were performed on $Fe_{2.8}V_{0.2}$, $Fe_{1.5}V_{1.5}$ and $FeVO_4$. In Fig. 8, the V *K*- and the Fe *K*-edge spectra are presented that were recorded in situ immediately before (0 min) and after (2 min) the reaction started as well as after

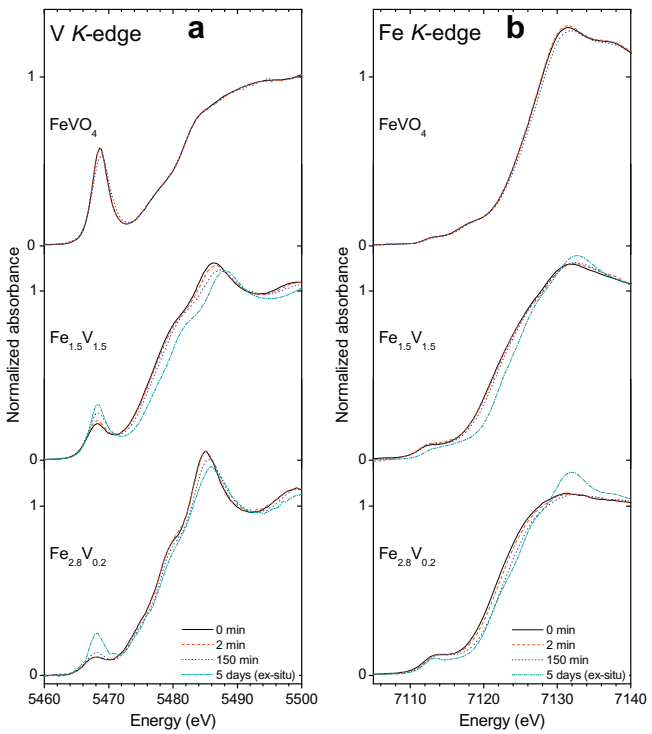

Fig. 8. (a) V *K*-edge and (b) Fe *K*-edge XANES spectra for $FeVO_4$, $Fe_{1.5}V_{1.5}$ and $Fe_{2.8}V_{0.2}$ as measured in situ after 0, 2 and 150 min and ex situ after 5 days on stream in methanol oxidation.

150 min on stream. In addition, to give information about the changes occurring over a longer period of time, complementary ex situ spectra recorded after 5 days in methanol oxidation are shown for $Fe_{2.8}V_{0.2}$ and $Fe_{1.5}V_{1.5}$.

Fig. 8 shows at the start of the in situ experiment (0 min) that the V *K*-edge positions ($E_{1/2}$) for $Fe_{2.8}V_{0.2}$, $Fe_{1.5}V_{1.5}$ and $FeVO_4$ are 5477.1, 5476.6 and 5480.8 eV, respectively and the Fe *K*-edge ($E_{1/2}$) positions are 7121.4, 7121.7 and 7124.3 eV, respectively, showing that both V and Fe in the spinel phase catalysts are less

oxidized than in $FeVO_4$. During methanol oxidation, both $Fe_{2.8}V_{0.2}$ and $Fe_{1.5}V_{1.5}$ show a shift of the V and Fe main edge position toward higher energies, revealing that both catalysts are oxidized during the reaction. Compared to the edge position at the start of the experiment, after 150 min on stream the shifts of the V *K*- and Fe *K*-edge positions ($E_{1/2}$) for $Fe_{2.8}V_{0.2}$ are +0.4 and +0.9 eV, respectively and for $Fe_{1.5}V_{1.5}$ the corresponding shifts are +0.5 and +0.4 eV, respectively. As shown by the ex situ spectra in Fig. 8, after 5 days on stream both the V and the Fe in the spinels have become even more oxidized. However, for $FeVO_4$ only negligible adjustments of the edge positions are observed after 150 min, indicating that the initial reduction of the catalyst is slower than the oxidation of the more reduced spinel phase catalysts.

Besides the shift of the V main edge position, on stream both the position and the intensity of the V pre-edge increase for $Fe_{2.8}V_{0.2}$ and $Fe_{1.5}V_{1.5}$. Since more accurate information regarding the valence and coordination can be extracted from both the V pre-edge and the Fe pre-edge, extended pre-edge analyses were performed according to the procedures previously described by Giuli et al. [35] and Chaurand et al. [37] for V and by Wilke et al. [38,39] for Fe. As shown in Fig. 9, for both $Fe_{1.5}V_{1.5}$ and $Fe_{2.8}V_{0.2}$ the normalized and background-subtracted V *K* pre-edge intensity increases with time on stream. As obtained from the spectra in Fig. 9, the centroid position and the pre-edge intensity are plotted in Fig. 10, where the values are compared with several reference compounds with known coordination and valence [35,37,40,41]. Since the spinel-type phase has four and six coordinated cation positions only, five coordinated positions are not likely to be found and hence, the results suggest for both catalysts that trivalent vanadium in octahedral positions $^{[VI]}V^{3+}$ is oxidized to predominantly tetravalent vanadium $^{[VI]}V^{4+}$ during the reaction. The lower initial value of both the centroid energy (5468.9 eV) and the intensity (0.10) for $Fe_{2.8}V_{0.2}$ compared to the values for $Fe_{1.5}V_{1.5}$ (5469.4 eV and 0.19, respectively) reveals that V is less oxidized in the former catalyst, confirming the TPO results in Fig. 7 and Table 1. However, as shown in Fig. 10, after five days in methanol oxidation vanadium in $Fe_{2.8}V_{0.2}$ has been oxidized to a slightly larger extent (+0.5 eV) than is the case in $Fe_{1.5}V_{1.5}$ (+0.3 eV), and the oxidation states have become more similar.

In Fig. 11 are the normalized and background-subtracted pre-edges of the Fe *K*-edge spectra for $Fe_{2.8}V_{0.2}$ and $Fe_{1.5}V_{1.5}$ presented that were recorded in situ after 0, 2 and 150 min use of the samples in methanol oxidation as well as the corresponding spectra recorded ex situ after five days on stream. All eight spectra are deconvoluted as a mixture of magnetite (Fe_3O_4) and maghemite (γ-Fe_2O_3) according to the number of peaks, relative positions and the FWHM reported by Wilke et al. [38]. Since the width of the experimental peak is too wide to be from magnetite only (peaks 1–3), a fourth peak significant for maghemite (peak 4) was added at higher energy. Consequently, in agreement with the TPO results in Fig. 7 and Table 1, the results reveal that neither

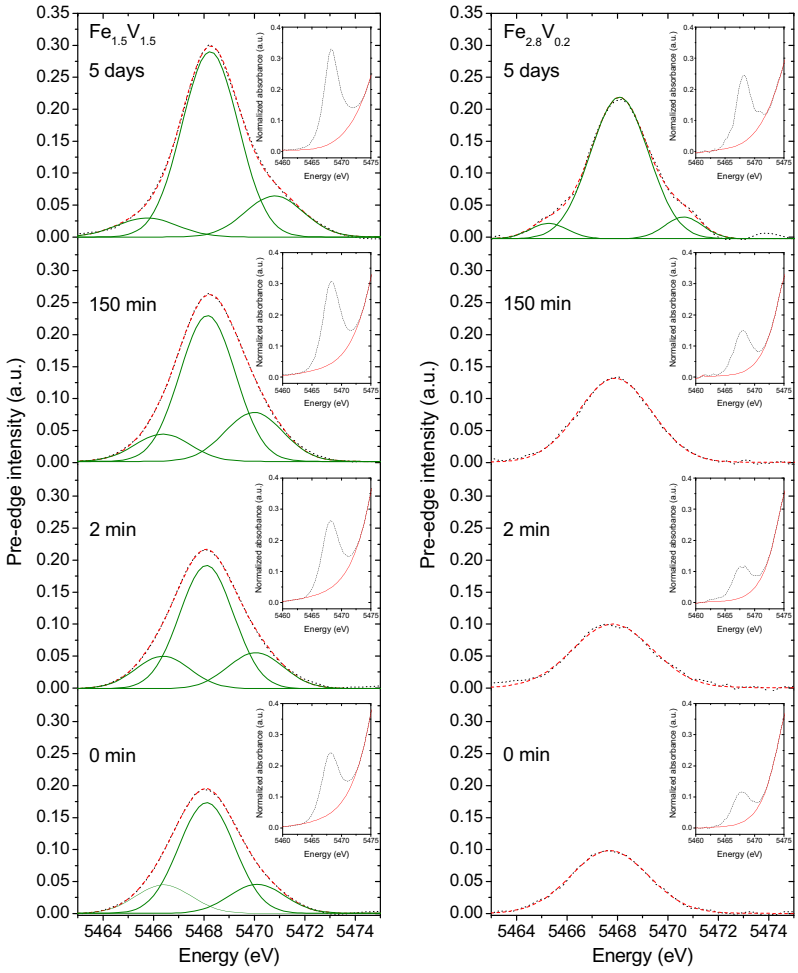

Fig. 9. Deconvolution of background-subtracted V *K* pre-peak spectra for $Fe_{2.8}V_{0.2}$ and $Fe_{1.5}V_{1.5}$ measured in situ after 0, 2 and 150 min and ex situ after five days on stream in methanol oxidation. The spectra are as obtained after subtracting the background contribution from the main edge (see inset spectra). As described in Ref. [37], the components have no obvious physical meaning but are used only for determining the centroid positions in Fig. 10.

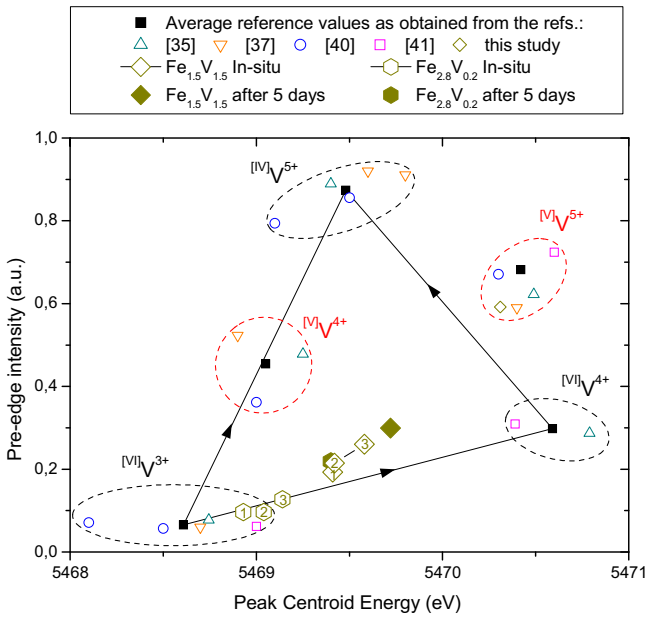

Fig. 10. Correlation between the intensity and the peak centroid energy of the background-subtracted V *K* pre-edge spectra for $Fe_{2.8}V_{0.2}$ and $Fe_{1.5}V_{1.5}$ as obtained from the spectra in Fig. 9. The data for the reference compounds are from Refs. [35,37,40,41], which have been intensity adjusted from Si(2 2 0) and Si(3 1 1) to Si(1 1 1) according to the difference given in Refs. [35,37]. The red dashed line surrounding the five coordinated reference samples marks unlikely positions since no such coordination is known to exist in the spinel structure [41]. The notations 1, 2 and 3 represent the centroid position and the intensity obtained in situ after 0, 2 and 150 min in methanol oxidation, respectively.

$Fe_{1.5}V_{1.5}$ nor $Fe_{2.8}V_{0.2}$ is a stoichiometric spinel but is partially oxidized. Also in agreement with the TPO results showing less oxidized cations in the fresh $Fe_{2.8}V_{0.2}$ than in the fresh $Fe_{1.5}V_{1.5}$ catalyst, the area contribution of peak 4 to the total peak area is 15.1% and 23.6%, respectively, revealing that the maghemite contribution, i.e. the number of cation vacancies is lower in $Fe_{2.8}V_{0.2}$ than in $Fe_{1.5}V_{1.5}$. After 150 min, the area fraction is 21.9% and 24.5%, respectively, and after five days on stream it increased to 30% and 41%, respectively, of the total peak area, revealing that during reaction the spinels become more and more oxidized and maghemite like.

To summarize, the XANES results reveal that although $Fe_{2.8}V_{0.2}$ as prepared is more reduced than $Fe_{1.5}V_{1.5}$, the spinel is still not stoichiometric, i.e. $Fe_{3-x}V_xO_4$. Instead, to some extent the structure has cation vacancies, explaining the maghemite-like Fe *K* pre-edge feature. During reaction, both the V and the Fe in $Fe_{2.8}V_{0.2}$ and $Fe_{1.5}V_{1.5}$ are oxidized resulting in even more maghemite-like structures with even more cation vacancies. Further, after five days in methanol oxidation, the valences of both V and Fe in the catalysts tend to more similar values. However, since the V content in $Fe_{1.5}V_{1.5}$ is considerably larger than in $Fe_{2.8}V_{0.2}$, in the reaction the former sample becomes more oxidized than the latter, resulting in a catalyst with higher concentration of cation vacancies.

3.5. XPS

XPS measurements were performed to determine the elemental composition and the oxidation states of the elements in the surface region. In Table 3 are gathered the bulk compositions of the prepared catalysts as designed and the surface compositions as determined by XPS before and after use of the catalysts in methanol oxidation. Compared to the bulk composition, the surface concentration of oxygen is considerably higher for all fresh and used spinel phase catalysts, showing that the surface is more oxidized than the bulk. Generally, the oxygen concentration at the surface is the highest for the used sample. For $FeVO_4$, on the other hand, the surface concentration of oxygen is more similar to the bulk value, which is in agreement with the cations in the bulk structure are being in their highest oxidation states. Except for $Fe_{1.5}V_{1.5}$ showing an excess of Fe compared to V at the surface, the data in Table 3 show that the V/Fe surface ratios for the fresh spinel samples largely agree with the respective bulk values. As seen in Fig. 12, after use in methanol oxidation of the spinels with low V/Fe bulk ratios ($Fe_{2.94}V_{0.06}$ and $Fe_{2.8}V_{0.2}$), the surface concentration of vanadium remains essentially unchanged. However, for the samples with higher bulk ratios ($Fe_{1.5}V_{1.5}$ and $Fe_{2.0}V_{1.0}$), a significant decrease in the surface concentration of vanadium is observed after the catalysis. Contrary to the data for the fresh spinel samples, the data in Table 3 show for the fresh $FeVO_4$ an enrichment of vanadium at the surface. However, after the catalysis the V/Fe ratio for $FeVO_4$ has decreased and tends to the same value as for the used $Fe_{1.5}V_{1.5}$ (0.57 and 0.53, respectively).

The oxidation state distributions of the cations were determined by resolution of the V $2p_{3/2}$ and Fe $2p_{3/2}$ peaks, which are shown in Figs. 13 and 14, respectively. Except for the fresh $Fe_{1.5}V_{1.5}$, all spinel samples show very similar oxidation state distribution of vanadium both as freshly prepared and respectively after use in methanol oxidation. As shown in Fig. 13, the V $2p_{3/2}$ peaks can be deconvoluted into three components with maxima at 517.2 ± 0.2 eV, 516.0 ± 0.2 eV and 515.0 ± 0.2 eV, which can be assigned to V^{5+}, V^{4+} and V^{3+}, respectively [23,25,45,46]. The oxidation state distribution obtained from the deconvolution is given in Table 4, showing for all freshly prepared spinel samples that V^{5+} is the predominating oxidation state (49–68%) followed by V^{4+} (23–33%) and V^{3+} (8–21%). After use in methanol oxidation, the samples become more oxidized with 72–78%, 18–24% and 1–6% of V^{5+}, V^{4+} and V^{3+}, respectively. The average oxidation number for V in the fresh and the used spinels is +4.39 and +4.72, respectively. As indicated also by the element composition presented in Table 3, showing a higher surface concentration of oxygen for the fresh $FeVO_4$ than for the spinels, the V $2p_{3/2}$ peak fitting reveals that only V^{5+} is present at the surface of the fresh $FeVO_4$. However, as shown in Fig. 13 and Table 4, after use of the samples in catalysis, the convoluted peaks are very similar for $FeVO_4$ and $Fe_{1.5}V_{1.5}$. The average oxidation number for V in the used $FeVO_4$ is +4.70, which is the same as the average oxidation number for the spinel samples.

Fig. 14 shows Fe $2p_{3/2}$ spectra for fresh and used catalysts. All used spinel-type catalysts show a Fe $2p_{3/2}$ peak at 711.0 ± 0.2 eV, revealing that Fe^{3+} is the only oxidation state present at the surface [23,25,47,48]. The spectra for the fresh catalysts, especially that for $Fe_{2.94}V_{0.06}$, additionally show a weak contribution from Fe^{2+} at the low energy side of the peak. For the fresh $FeVO_4$ the peak position is 711.8 eV, which is 0.7 eV higher than for the used sample. This difference does not seem to be due to reduction of the sample during the catalysis. Rather, the shift is due to the transformation of triclinic $FeVO_4$ to a spinel-type structure since the binding energy for the used $FeVO_4$ (711.1 eV) is only 0.1 eV above the average binding energy for the spinel samples with Fe^{3+} surface states. This transformation is in line with the XRD results in Fig. 2, showing transformation of the triclinic $FeVO_4$ to a spinel-type phase.

3.6. Catalytic performance and volatility of active metals

In Table 5 are gathered the areal and the specific activities for the fresh catalysts and the corresponding samples after they have been used in methanol oxidation for 5 days. In general, the activities of the different catalysts are in the same order of magnitude, and besides for $FeVO_4$, the difference in activity between fresh and used samples is relatively small. Of the fresh samples, $FeVO_4$ is more active than the spinels. Among the spinels, $Fe_{2.94}V_{0.06}$

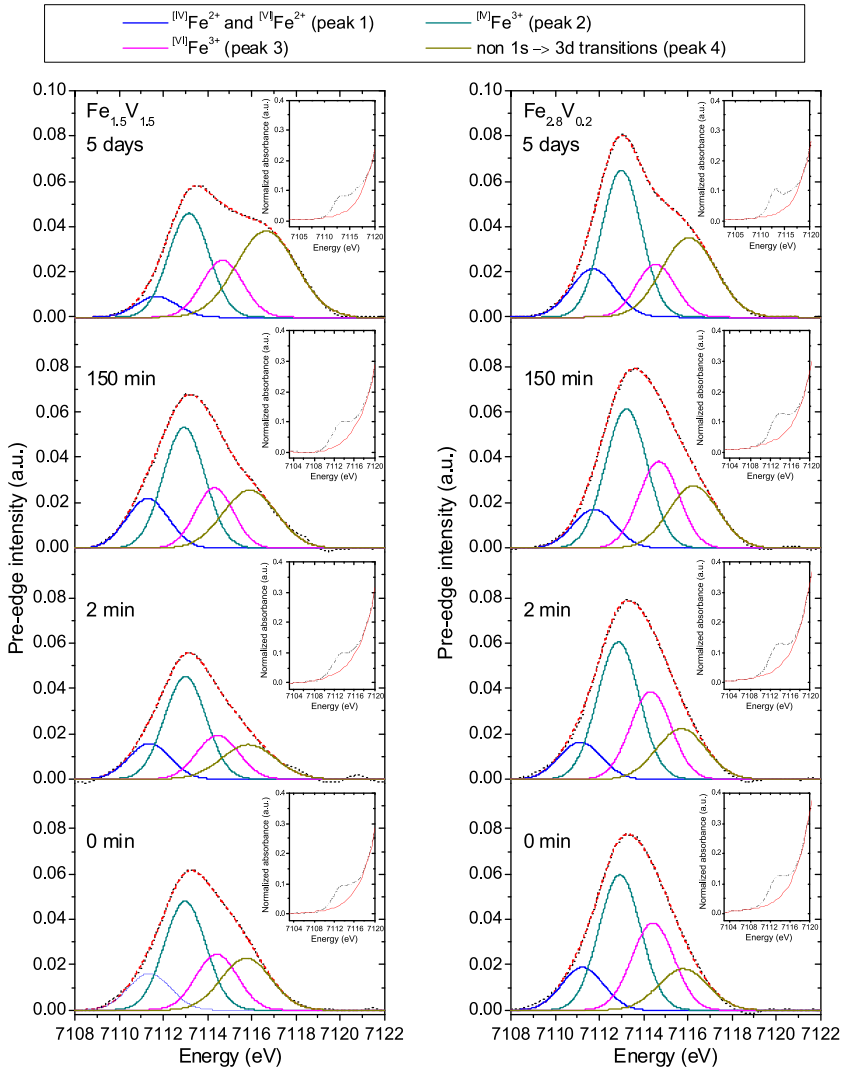

Fig. 11. Peak deconvolution of background-subtracted Fe *K* pre-peak spectra for $Fe_{2.8}V_{0.2}$ and $Fe_{1.5}V_{1.5}$ recorded in situ after 0, 2 and 150 min and ex situ after five days on stream in methanol oxidation. The spectra are as obtained after subtracting the background contribution from the main edge (see inset spectra). All spectra have been deconvoluted as a mixture of magnetite and maghemite according to the deconvolutions presented in Ref. [38].

Table 3
Bulk composition of the catalysts and the surface composition as determined by XPS.

Sample	Bulk composition[a] (at%)				XPS fresh catalyst (at%)				XPS used catalyst (at%)			
	Fe	V	O	V:Fe	Fe	V	O	V:Fe	Fe	V	O	V:Fe
$FeVO_4$[a]	16.7	16.7	66.7	1.00	12.2	18.6	69.2	1.52	18.3	10.4	71.3	0.57
$Fe_{1.5}V_{1.5}$	20.3	20.3	59.4	1.00	16.5	11.6	71.9	0.70	20.2	10.7	69.2	0.53
$Fe_{2.0}V_{1.0}$	28.1	14.0	57.9	0.50	21.9	10.5	67.6	0.48	22.5	7.1	70.5	0.32
$Fe_{2.8}V_{0.2}$	39.0	2.8	58.3	0.07	30.1	2.1	67.9	0.07	24.3	3.2	72.5	0.13
$Fe_{2.94}V_{0.06}$	41.7	0.9	57.5	0.02	29.6	1.4	69	0.05	27.7	1.5	70.8	0.05
$Fe_{3.0}V_{0.0}$	42.8	0	57.2	0.00	30.5	0	69.5	0.00	N.D.[b]	N.D.	N.D.	0.00

[a] Metal composition as designed in the synthesis and oxygen composition as determined by TPO.
[b] Not determined.

and $Fe_{1.5}V_{1.5}$ have the highest areal and specific activity, respectively. The addition of a small amount of V to the Fe_3O_4 spinel base strongly enhances the activity as comparison of the data for $Fe_{3.0}V_{0.0}$ and $Fe_{2.94}V_{0.06}$ shows. However, further addition of V does not increase but rather decrease the areal activity, whereas the specific activity increases due to the specific surface area increases (Table 1).

For all prepared catalysts, the selectivity to formaldehyde and by-products at 90% methanol conversion are displayed in Fig. 15. Except for $Fe_{3.0}V_{0.0}$ and $Fe_{2.94}V_{0.06}$ producing mainly carbon oxides, formaldehyde is the main product being formed over the samples. Although the atomic V/Fe ratio is the same for $FeVO_4$ and the spinel phase $Fe_{1.5}V_{1.5}$, the latter sample shows significantly lower selectivity to formaldehyde reaching only ~70% compared to ~90% for $FeVO_4$. However, as the fraction of V in the spinel phase is decreased, the selectivity to formaldehyde increases and tends to a maximum of about 91% for $Fe_{2.8}V_{0.2}$. For all samples, the primary by-products are carbon oxides (CO_x) followed by smaller amounts

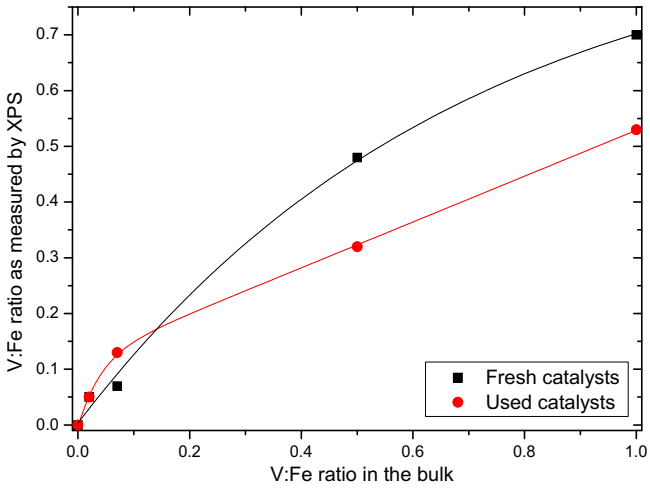

Fig. 12. The V/Fe ratio as measured by XPS in fresh respectively used catalysts as a function of the V/Fe ratio in the bulk.

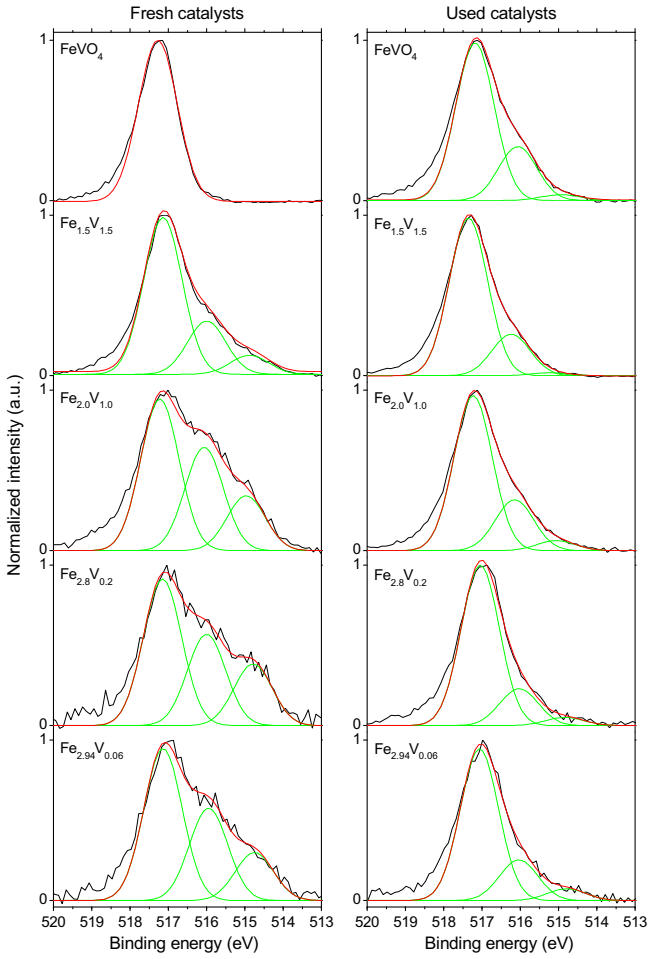

Fig. 13. Deconvolution of V $2p_{3/2}$ XPS spectra recorded before and after use of the samples in methanol oxidation, showing the oxidation state distribution of vanadium in fresh (left) and used (right) catalysts.

of methyl formate (MF) and dimethyl ether (DME). Between the samples, the selectivity to CO_x varies strongly and generally is high for the samples showing poor selectivity to formaldehyde.

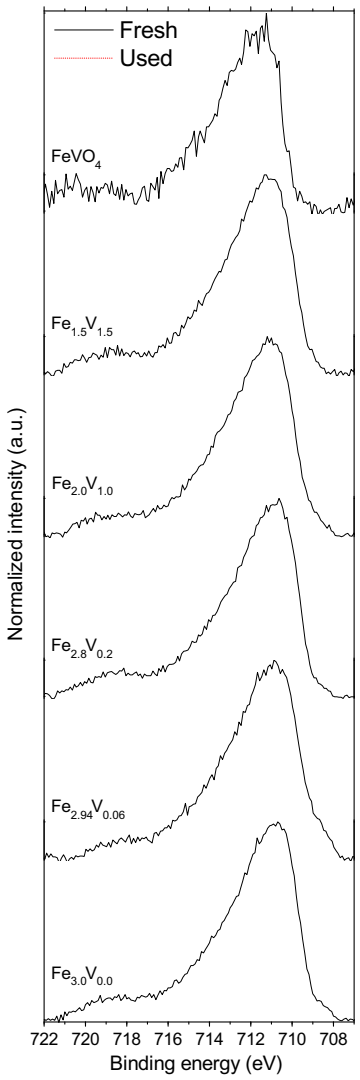

Fig. 14. Fe $2p_{3/2}$ XPS spectra recorded before (fresh) and after use of the samples in methanol oxidation (used).

To determine the volatility of vanadium in methanol oxidation, the elemental composition of the catalysts was measured by ICP before and after five days on stream at differential conditions at 300 °C. As displayed in Table 6, the metal composition of the prepared catalyst agrees with the designed composition. The spinel phase catalysts show no notable difference in composition after the samples being subjected to methanol oxidation for five days. For $FeVO_4$, on the other hand, a loss of 8% of the vanadium is observed similar to what has been reported earlier [25]. The relatively stable metal composition of the spinel-type catalysts is confirmed by the activity data in Table 5, showing almost no deactivation of the spinel samples. However, a considerably deactivation of the $FeVO_4$ sample is observed, showing similar areal activity as $Fe_{1.5}V_{1.5}$ after five days on stream in agreement with a spinel-type structure being formed (see Fig. 2).

4. Discussion

Our investigation has demonstrated that the Fe–V–oxide spinel-type catalysts are interesting as selective oxidation catalysts in view of several aspects. One important factor in methanol oxidation is that they are stable with regard to volatilization of the active metal, which is substantially lower compared to the volatilization

Table 4
Oxidation state distribution and average oxidation number of the vanadium at the surface region on both fresh and used catalysts as determined by deconvolution of the V $2p_{3/2}$ peak.

Sample	Fresh sample			Used sample			Average oxidation number	
	V^{5+}	V^{4+}	V^{3+}	V^{5+}	V^{4+}	V^{3+}	Fresh	Used
$FeVO_4$	100	0	0	73	25	3	5.00	4.70
$Fe_{1.5}V_{1.5}$	68	23	8	78	21	1	4.60	4.77
$Fe_{2.0}V_{1.0}$	49	33	18	72	24	5	4.31	4.67
$Fe_{2.8}V_{0.2}$	49	30	21	78	18	4	4.28	4.74
$Fe_{2.94}V_{0.06}$	52	32	16	74	20	6	4.36	4.69

Table 5
Activity of fresh and used samples.

Sample	Areal activity (μmol/m^2, s)[a]		Specific activity (μmol/g, s)[b]	
	Fresh samples[c]	Used samples[d]	Fresh samples[c]	Used samples[d]
$FeVO_4$	2.9	1.8	44.1	29.3
$Fe_{1.5}V_{1.5}$	1.4	1.5	25.2	23.3
$Fe_{2.0}V_{1.0}$	1.6	1.6	22.6	18.4
$Fe_{2.8}V_{0.2}$	1.6	1.7	12.6	11.7
$Fe_{2.94}V_{0.06}$	2.3	2.7	13.1	11.4
$Fe_{3.0}V_{0.0}$	1.0	N.D.[e]	5.3	N.D.

[a] Areal activity = (Molar methanol flow rate × Differential conversion):(Catalyst mass × Specific surface area).
[b] Specific activity = (Molar methanol flow rate × Differential conversion):Catalyst mass.
[c] Samples as prepared after stabilization for about 2 h.
[d] Samples after 5 days in methanol oxidation.
[e] Not determined.

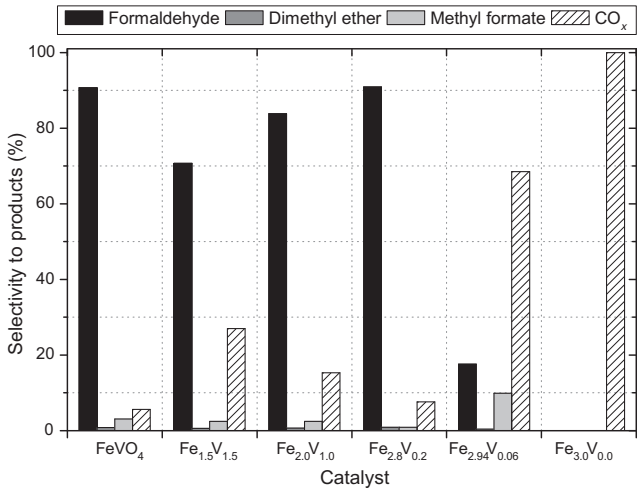

Fig. 15. Selectivity to formaldehyde, dimethyl ether, methyl formate and carbon oxides at 90% conversion of methanol. The data are for steady-state conditions at 300 °C with an inlet concentration of methanol and air of 10 vol.% each.

Table 6
Designed composition of the catalysts and the composition determined by ICP analysis of the catalysts as prepared and after 5 days use in methanol oxidation.

Sample	Composition as designed		ICP fresh catalyst		ICP used catalyst	
	Fe	V	Fe	V	Fe	V
$FeVO_4$	0.50	0.50	0.51	0.49	0.53	0.47
$Fe_{1.5}V_{1.5}$	0.50	0.50	0.49	0.51	0.49	0.51
$Fe_{2.0}V_{1.0}$	0.67	0.33	0.67	0.33	0.65	0.35
$Fe_{2.8}V_{0.2}$	0.93	0.07	0.93	0.07	0.93	0.07
$Fe_{2.94}V_{0.06}$	0.98	0.02	0.98	0.02	0.98	0.02
$Fe_{3.0}V_{0.0}$	1.00	0.00	N.D.[a]	N.D.	N.D.	N.D.

[a] Not determined.

of Mo from the commercial $MoO_3/Fe_2(MoO_4)_3$-type catalyst [25]. An important property here is that the spinel structure is flexible and allows the cations to be in different oxidation states and to change oxidation state within the same basic structure type retaining the ratio between the metals [26,49–52]. Opposed to the Fe–V–O spinel catalysts, many other transition metal oxide phases transform into new phases when the rate of oxygen consumption differs from the rate of reoxidation. Examples here are the vanadium oxide system when being used for the ammoxidation of 3-picoline [53]. Also in binary and multicomponent oxide systems, new phases can form depending on the reaction conditions, for example in methanol oxidation $Fe_2(MoO_4)_3$ may transform to $FeMoO_4$ with a different Mo/Fe ratio and MoO_3 [7,10]. In tubular reactors, both the surface and the phase composition may change along the catalytic bed due to the composition of the reacting gas and possibly the reaction temperature changes, giving more complex dependences of the reaction kinetics [54]. Therefore, in applications it is more preferable to have a phase stable catalyst since it gives more stable operation and simplifies the kinetic models being used for the design of load plans.

The fact that the Fe–V–oxide spinel structure is a stable phase in methanol oxidation is confirmed by the XRD results in Fig. 2 and Table 2, showing no formation of any new type of structure for the spinel phases after 5 days use in methanol oxidation. Although XRD (Fig. 2) and HRTEM imaging (Fig. 4) in a few cases show lower crystallinity of the spinel samples after they have been used in methanol oxidation, almost no changes are observed in either specific surface area (Table 1), particle size (Fig. 3) or activity (Table 5). The flexibility of the spinel-type structure is due to its ability to form cation vacancies. For instance, both magnetite Fe_3O_4 and maghemite γ-Fe_2O_3 have spinel structures where the former with both Fe^{2+} and Fe^{3+} has no vacancies, whereas in the latter structure, which can be written $Fe_{8/3}\square_{1/3}O_4$ with exclusively Fe^{3+}, one-ninth of the metal positions (11.1%) are vacant [43]. It is well known that some of the iron in Fe_3O_4 can be substituted with vanadium [26,49–52,55,56]. The structural formula for stoichiometric $Fe_{3-x}V_xO_4$ spinels with $0 \leqslant x \leqslant 2$ has been expressed in more detail as $(Fe^{2+}_{\alpha}Fe^{3+}_{1-\alpha})_A(Fe^{2+}_{1-\alpha}Fe^{3+}_{1-\alpha}V^{3+}_{x})_BO^{2-}_4$ with $\alpha = x/2$ and tetrahedral (A) and octahedral (B) sites [49]. Thermal studies of this type of spinel phase have demonstrated that oxidation of Fe^{2+} and V^{3+} to give Fe^{3+} and V^{5+} via V^{4+}, respectively, is possible with preservation of the basic spinel-type structure by forming cation vacancies to maintain electroneutrality [26,49,51,52]. Our results agree with these findings in that XRD shows that the spinel structure is stable in methanol oxidation simultaneously as XANES shows that both vanadium (Figs. 8 and 10) and iron (Figs. 8 and 11) are being oxidized. The data points in Fig. 10 for $Fe_{1.5}V_{1.5}$ and $Fe_{2.8}V_{0.2}$ show for both catalysts incomplete oxidation of octahedrally coordinated vanadium from the trivalent to the tetravalent state. The slight deviation of the data points from the straight line representing the transition of octahedral V^{3+} to form octahedral V^{4+} indicates that the latter species is in a more distorted octahedral configuration rather than some V^{5+} should form. The distortion occurring as a result of the oxidation is likely associated with the simultaneous

formation of cation vacancies, resulting in shortening of some of the metal–oxygen bonds. Compared with the V-rich samples, the observed higher stability in methanol oxidation of the bulk of the V-poor catalysts (Figs. 2 and 4–6) can be explained by the cation vacancies here being more ordered. Although the $Fe_{1.5}V_{1.5}$ sample after 5 days use in methanol oxidation is more oxidized than the used $Fe_{2.8}V_{0.2}$ and therefore contains more cation vacancies, the HRTEM (Figs. 4–6) and XRD (Table 2) characterization reveal that only the latter sample shows ordering of the vacancies. However, since neither of the two samples in freshly prepared form show any superstructure reflections, although both contain cation vacancies (Table 1), it can be concluded that also in the V-poor $Fe_{2.8}V_{0.2}$ catalyst the vacancies can be disordered when being present in low concentration.

Concerning the composition of the catalyst surfaces, the XPS data in Table 3 indicate for $Fe_{1.5}V_{1.5}$ and $Fe_{2.0}V_{1.0}$ some volatilization of V during the catalysis, whereas no change is observed for the samples with lower vanadium contents. Considering the fact that the ICP analysis data in Table 6 for the bulk clearly show that the spinel catalysts are stable in methanol oxidation, the loss of V from $Fe_{1.5}V_{1.5}$ and $Fe_{2.0}V_{1.0}$ possibly is confined to the surface or the nearby region and does not proceed into the bulk. Previously, it has been demonstrated for supported V- and Fe–V–oxide catalysts that iron stabilizes the vanadium in methanol oxidation restricting its volatilization [25]. Therefore, it can be suggested that the loss of vanadium from $Fe_{1.5}V_{1.5}$ and $Fe_{2.0}V_{1.0}$ takes place only over an initial period, during which an iron-rich surface is formed. The fact that this period is short is in line with the fresh and the used samples having similar activity (Table 5). Surrounded by Fe, the V atoms then become significantly less volatile and consequently the vanadium loss rate is declining. The stabilizing effect of Fe on the volatility has been shown also in the Fe–Mo–oxide system, in which the molybdenum in the $Fe_2(MoO_4)_3$ phase is considerably less volatile than in MoO_3 [10]. Compared to the spinel catalysts, the data in Tables 3 and 6 for $FeVO_4$ show greater changes, which partially is associated with its transformation into the spinel-type structure. Compared with the vanadium-rich samples, the vanadium-poor samples $Fe_{2.94}V_{0.06}$ and $Fe_{2.8}V_{0.2}$ show smaller difference between the bulk and surface compositions both before and after use in the reaction (see Fig. 12). Thus, a smaller difference is in agreement with XRD (Fig. 2) and HRTEM (Figs. 4–6) showing higher stability of the vanadium-poor catalysts.

The XPS data for vanadium in Fig. 13 and Table 4 show for the spinel samples contributions from V^{5+}, V^{4+} and V^{3+} in decreasing amounts for both fresh and used samples. The corresponding spectra for iron in Fig. 14 show that iron is mainly trivalent at the surface. Moreover, there is a general tendency that the spinel samples are more oxidized after being used in methanol oxidation. Also, compared with the XANES data for V (Fig. 10) and Fe (Fig. 11) in the bulk, the surfaces of the spinel catalysts are in a more oxidized form. A more oxidized surface region, preserving the spinel-type structure, does not cause any structural breakdown since the oxidation creates cation vacancies that are accommodated in the structure [26,49–52]. The HRTEM images in Figs. 3–6 and recorded diffraction patterns support that the basic spinel-type structure is stable.

The activity data in Table 5 show stable behavior of the Fe–V–O spinel catalysts. Almost no difference in areal activity is notable after stabilization of the samples for 2 h compared to after 5 days use in methanol oxidation, in spite of the XANES results in Figs. 8–11 clearly demonstrate that gradual oxidation of the bulk takes place during this period of time. Such behavior suggests that the surfaces are equilibrated relatively fast compared to the bulk and are stable. However, expressing the activity per mass unit, the values in Table 5 show a minor decrease in specific activity with use of the samples in methanol oxidation. The decrease is due to the decrease in surface area that is notable in Table 1, although imaging by TEM (Fig. 3) does not reveal any difference in particle size between the fresh and the used catalysts. In agreement with the XRDs in Fig. 2 showing transformation of $FeVO_4$ into a spinel-type structure, the areal activity values in Table 5 for the used $FeVO_4$ and $Fe_{1.5}V_{1.5}$ are almost the same. Moreover, the areal activities of $Fe_{1.5}V_{1.5}$, $Fe_{2.0}V_{1.0}$ and $Fe_{2.8}V_{0.2}$ are almost identical, which could suggest that the surfaces of the spinel phases consist of a monolayer of vanadia. In the literature, experimental results have previously been reported, suggesting that the surfaces of bulk metal vanadates may consist of a vanadia layer [20]. However, neither the fact that $Fe_{2.94}V_{0.06}$ clearly shows higher areal activity than $Fe_{2.8}V_{0.2}$, $Fe_{2.0}V_{1.0}$ and $Fe_{1.5}V_{1.5}$ nor the element compositions of the near surface regions as determined by XPS (Fig. 12 and Table 3) give any support for the surfaces of the spinel catalysts should consist exclusively of a monolayer of vanadium oxide. Rather, the similar activity of the latter samples is a combination of they have diverse distribution of differently coordinated vanadia with dissimilar activity and selectivity as indicated by the selectivities of the samples in Fig. 15 for high methanol conversion. The observation that $Fe_{2.94}V_{0.06}$ with the lowest vanadium content is more active per surface area unit than both Fe_3O_4 ($Fe_{3.0}V_{0.0}$) and the samples with higher vanadium contents could possibly indicate that isolated vanadia species are more active than polymeric vanadia and polymeric iron oxide species. In fact, a similar finding has been reported for the partial oxidation of methane on silica-supported vanadia, where monomeric vanadia was concluded to be the most active structure [57]. However, considering for $Fe_{2.8}V_{0.2}$ that the V/Fe surface ratio is only ~0.10 (see Table 3), it seems that also this sample with lower activity than $Fe_{2.94}V_{0.06}$ should expose monomeric vanadia species. Therefore, the high activity of $Fe_{2.94}V_{0.06}$ more likely can be due to the addition of a small amount of vanadium to the Fe_3O_4 base causes doping of the iron sites, making them more active (Table 5) but still unselective to formaldehyde (Fig. 15).

The selectivity data in Fig. 15 for the $Fe_{3-x-y}V_x\square_yO_4$ series of samples, showing that the selectivity to formaldehyde at 90% methanol conversion passes through a maximum and is the highest 91% for $Fe_{2.8}V_{0.2}$, are in line with the site isolation hypothesis. Clearly, the results suggest the existence of an optimal V/Fe metal ratio, at which spatially separated active centers with a restricted number of reacting oxygen give the highest selectivity [58–60]. Thus, a low concentration of vanadium eliminates active but non-selective Fe–O–Fe centers existing on $Fe_{3.0}V_{0.0}$, forming instead highly selective Fe–O–V centers. At higher concentrations, less selective polymeric vanadium centers (V–O–V) are formed at the expense of monomeric vanadium centers (Fe–O–V) [23].

Fig. 15 shows a considerable difference in the selectivity to formaldehyde between $FeVO_4$ and $Fe_{1.5}V_{1.5}$, in spite of the samples giving similar XRD patterns after being used in methanol oxidation (Fig. 2). Here, it should be noted that the samples used in the characterizations were subjected to methanol oxidation at differential conditions (see Section 2.3.), i.e. with almost unchanged partial pressures of the reactants along the bed. At the same conditions, the reaction rates (Section 2.2.) were measured in agreement with the areal activity of the used $FeVO_4$ tends to that for $Fe_{1.5}V_{1.5}$ (Table 5). However, the selectivity data in Fig. 15 are for high methanol conversion, requiring longer residence time. At these conditions, the $FeVO_4$ sample obviously transforms into a spinel structure in the first part of the catalytic bed as Fig. 2 shows, whereas it remains triclinic $FeVO_4$ in lower parts as previously has been shown by XRD of a sample being used at high methanol conversion [23].

Since the commercial $MoO_3/Fe_2(MoO_4)_3$-type catalyst presently being used in the production of formaldehyde suffers from volatilization of molybdenum [6–10], alternative more stable catalysts

are of interest only if they show at least comparable selectivity to formaldehyde. According to these requirements, the $Fe_{2.8}V_{0.2}$ catalyst shows promising results with ~91% selectivity to formaldehyde at high methanol conversion (Fig. 15), and no notable volatility of vanadium at relevant reaction conditions i.e. 300 °C and 10 vol.% each of methanol and oxygen in the feed (Table 6). For comparison, the selectivity over a commercial $MoO_3/Fe_2(MoO_4)_3$-type catalyst is ~93% [23,25], and the volatility of the latter is considerably higher, showing a decrease of the Mo/Fe ratio from 2.2 to 1.4 when measured at the same conditions as has been used in the present work [25]. Concerning the activity, the data in Table 5 show $Fe_{2.8}V_{0.2}$ to have similar areal activity as $FeVO_4$, which according to our previous work [23] is less than a factor two more active in the same units than the molybdate catalyst. Moreover, with a V/Fe metal ratio equal to 0.07, the relatively low amount of vanadium in the $Fe_{2.8}V_{0.2}$ catalyst in combination with low volatility makes it more environmentally attractive than other vanadates studied for methanol oxidation, which typically have V/co-metal ratios ranging from 0.7 to 1 [11,13–15,20,21,23]. $Fe_{2.8}V_{0.2}$ shows a selectivity to formaldehyde that is comparable to that of $FeVO_4$ (Fig. 15), but in favor of $Fe_{2.8}V_{0.2}$ is that it is less volatile (Table 6) and contains significantly less amount of harmful vanadium. However, still it is not as selective as the commercial type $MoO_3/Fe_2(MoO_4)_3$ catalyst. Consequently, unless the selectivity is improved, the $Fe_{2.8}V_{0.2}$ spinel catalyst cannot replace the $MoO_3/Fe_2(MoO_4)_3$ catalyst without rising the methanol cost, which of course has to be considered in relation to other costs and earnings.

5. Conclusions

Cation vacant $Fe_{3-x-y}V_x\square_yO_4$ spinel-type catalysts are interesting oxidation catalysts in view of the spinel structure being flexible allowing the cations to be in different oxidation states and to change oxidation state within the same basic structure, maintaining electroneutrality through adjustment of the number of cation vacancies.

Opposed to the industrial-type $MoO_3/Fe_2(MoO_4)_3$ catalyst showing volatility of Mo, the $Fe_{3-x-y}V_x\square_yO_4$ spinel phases are stable in methanol oxidation showing no volatility of the metals.

The $Fe_{3-x-y}V_x\square_yO_4$ spinel phases are active for methanol oxidation. Phases with V/Fe ratios from 0.07 to 1.0 have similar areal activity but different selectivity to formaldehyde. Varying the V/Fe ratio from 0 to 1, the best performing composition is V/Fe = 0.07, giving 91% selectivity to formaldehyde at high methanol conversion. Samples with higher and lower V/Fe ratio are less selective. The results indicate that monomeric vanadium sites surrounded by iron (Fe–O–V) are highly selective, whereas polymeric vanadium and iron centers (V–O–V and Fe–O–Fe) are less selective.

Acknowledgments

The Swedish Research Council (VR) is acknowledged for financial support. Parts of the research were carried out at beamline I811, MAX-lab synchrotron radiation source, Lund University, Sweden. Funding for the beamline I811 project was kindly provided by The Swedish Research Council and The Knut and Alice Wallenberg Foundation.

References

[1] B. Crichton, in: Informally Speaking (newsletter from Perstorp Formox, <http://www.perstorpformox.com>), autumn/winter 2009, pp. 4–5.
[2] G. Reuss, W. Disteldorf, A.O. Gamer, A. Hilt, Ullmann's Encyclopedia of Industrial Chemistry, seventh ed., vol. A11, Wiley-VCH, Weinheim, 2008, pp. 619–652.
[3] H.R. Gerberich, G.C. Seaman, Kirk–Othmer Encyclopedia of Chemical Technology, vol. 12, John Wiley & Sons, 2009, pp. 107–128.
[4] B. Crichton, in: Informally Speaking (newsletter from Perstorp Formox, <http://www.perstorpformox.com>), spring/summer 2003, pp. 12–13.
[5] Methanex Corporation, Vancouver, Canada (methanol prizes from 2002 to 2008, <http://www.methanex.com>).
[6] B.I. Popov, V.N. Bibin, G.K. Boreskov, Kinet. Catal. 17 (1976) 371–377. Eng. Transl.
[7] N. Burriesci, F. Garbassi, M. Petrera, G. Petrini, N. Pernicone, in: B. Delmon, G.F. Froment (Eds.), Catalyst Deactivation, Elsevier, Amsterdam, 1980, pp. 115–126.
[8] A.P.V. Soares, M.F. Portela, A. Kiennemann, J.M.M. Millet, React. Kinet. Catal. Lett. 75 (2002) 13–20.
[9] A.P.V. Soares, M.F. Portela, A. Kiennemann, L. Hilaire, Chem. Eng. Sci. 58 (2003) 1315–1322.
[10] A. Andersson, M. Hernelind, O. Augustsson, Catal. Today 112 (2006) 40–44.
[11] I.E. Wachs, L.E. Briand, US Patent 7 193 117 B2, 2007, to Lehigh University.
[12] J. Holmberg, Perstorp Formox, personal communication.
[13] P. Forzatti, E. Tronconi, A.S. Elmi, G. Busca, Appl. Catal. A 157 (1997) 387–408.
[14] R. Maliński, React. Kinet. Catal. Lett. 5 (1976) 265–271.
[15] R. Maliński, M. Akimoto, E. Echigoya, J. Catal. 44 (1976) 101–106.
[16] G. Deo, I.E. Wachs, J. Haber, Crit. Rev. Surf. Chem. 4 (1994) 141–187.
[17] G. Deo, I.E. Wachs, J. Catal. 146 (1994) 323–334.
[18] S. Lim, G.L. Haller, Appl. Catal. A 188 (1999) 277–286.
[19] X. Gao, I.E. Wachs, Top. Catal. 18 (2002) 243–250.
[20] L.E. Briand, J-M. Jehng, L. Cornaglia, A.M. Hirt, I.E. Wachs, Catal. Today 78 (2003) 257–268.
[21] G.V. Isaguliants, I.P. Belomestnykh, Catal. Today 100 (2005) 441–445.
[22] T. Kim, I.E. Wachs, J. Catal. 255 (2008) 197–205.
[23] R. Häggblad, J.B. Wagner, S. Hansen, A. Andersson, J. Catal. 258 (2008) 345–355.
[24] H. Zhang, Z. Liu, Z. Feng, C. Li, J. Catal. 260 (2008) 295–304.
[25] R. Häggblad, M. Massa, A. Andersson, J. Catal. 266 (2009) 218–227.
[26] V. Nivoix, B. Gillot, Solid State Ionics 111 (1998) 17–25.
[27] D. Aymes, N. Millot, V. Nivoix, P. Perriat, B. Gillot, Solid State Ionics 101–103 (1997) 261.
[28] S. Denis, E. Baudrin, M. Touboul, J.-M. Tarascon, J. Elecrochem. Soc. 144 (1997) 4099–4109.
[29] Informally Speaking (newsletter from Perstorp Formox, <http://www.perstorpformox.com>), spring/summer 2010, pp. 9–10.
[30] C. Sejrbo Nielsen, N. Knudsen, Chem. Eng. 757 (2004) 26–27.
[31] B. Robertson, E. Kostiner, J. Solid State Chem. 4 (1972) 29–37.
[32] M.E. Fleet, Acta Crystalogr. B37 (1981) 917–920.
[33] Z. Somogyvári, E. Sváb, G. Mészáros, K. Krezhov, I. Nedkov, I. Sajó, F. Bourée, Appl. Phys. A74 (2002) S1077–S1079 (Suppl.).
[34] S. Kraft, J. Stumpel, P. Becker, U. Kuetgens, Rev. Sci. Instrum. 67 (1996) 681–687.
[35] G. Giuli, E. Paris, J. Mungall, C. Romano, D. Dingwell, Am. Mineral. 89 (2004) 1640–1646.
[36] S.R. Sutton, J. Karner, J. Papike, J.S. Delaney, C. Shearer, M. Newville, P. Eng, M. Rivers, M.D. Dyar, Geochim. Cosmochim. Acta 69 (2005) 2333–2348.
[37] P. Chaurand, J. Rose, V. Briois, M. Salome, O. Proux, V. Nassif, L. Olivi, J. Susini, J.L. Hazemann, J.Y. Bottero, J. Phys. Chem. B 111 (2007) 5101–5110.
[38] M. Wilke, F. Farges, P.E. Petit, G.E. Brown Jr., F. Martin, Am. Mineral. 86 (2001) 714–730.
[39] P.E. Petit, F. Farges, M. Wilke, V.A. Solé, J. Synchotron. Rad. 8 (2001) 952–954.
[40] O.V. Safonova, M. Florea, J. Bilde, P. Delichere, J.M.M. Millet, J. Catal. 268 (2009) 156–164.
[41] J. Wong, F.W. Lytle, R.P. Messmer, D.H. Maylotte, Phys. Rev. B 30 (1984) 5596–5610.
[42] JCPDS International Centre for Diffraction data, Powder Diffraction File, Swarthmore, PA, 1991.
[43] K.J. Kim, S. Choi, Y.R. Park, J.H. Lee, J.Y. Park, S.J. Kim, J. Magn. Magn. Mater. 310 (2007) e876–e877.
[44] E.N. Maslen, V.A. Streltsov, N.R. Streltsova, N. Ishizawa, Acta Crystallogr. B50 (1994) 435–441.
[45] S.L.T. Andersson, S. Järås, J. Catal. 64 (1980) 51–67.
[46] L. O'Mahony, T. Curtin, D. Zemlyanov, M. Mihov, B.K. Hodnett, J. Catal. 227 (2004) 270–281.
[47] E. Baba Ali, J.C. Bernède, A. Barreau, Mater. Chem. Phys. 63 (2000) 208–212.
[48] K. Asami, K. Hashimoto, Corros. Sci. 17 (1977) 559–570.
[49] B. Gillot, V. Nivoix, Mater. Res. Bull. 34 (1999) 1735–1747.
[50] V. Nivoix, B. Gillot, Chem. Mater. 12 (2000) 2971–2976.
[51] V. Nivoix, B. Gillot, Mater. Chem. Phys. 63 (2000) 24–29.
[52] B. Gillot, M. Nohair, Phys. Status Solidi A 176 (1999) 1047–1060.
[53] A. Andersson, J.-O. Bovin, P. Walter, J. Catal. 98 (1986) 204–220.
[54] A. Bielański, J. Haber, Oxygen in Catalysis, Marcel Dekker, New York, 1991 (Chapter 4) pp. 169–177.
[55] M. Wakihara, Y. Shimizu, T. Katsura, J. Solid State Chem. 3 (1971) 478–483.
[56] D.B. Rogers, R.J. Arnott, A. Wold, J.B. Goodenough, J. Phys. Chem. Solids 24 (1963) 347–360.
[57] L.D. Nguyen, S. Loridant, H. Launay, A. Pigamo, J.L. Dubois, J.M.M. Millet, J. Catal. 237 (2006) 38–48.
[58] J.L. Callahan, R.K. Grasselli, AIChE J. 9 (1963) 755–760.
[59] A. Andersson, S. Hansen, A. Wickman, Top. Catal. 15 (2001) 103–110.
[60] R.K. Grasselli, Catal. Today 99 (2005) 23–31.